

## **Magneto-Structural Characterization of Strontium Substituted Lead Hexaferrite**

A. L. Guerrero Serrano, S. A. Palomares-Sánchez, M. Mirabal-García, J. A. Matutes-Aquino

### **Abstract**

In this work, the magnetic and structural properties of the system  $\text{Pb}_{1-x}\text{Sr}_x\text{Fe}_{12}\text{O}_{19}$  ( $x = 0.1, 0.3, 0.5, 0.7$  and  $0.9$ ) are reported. The samples were prepared by the traditional ceramic method. All the compounds are isostructural with the strontium hexaferrite ( $\text{SrFe}_{12}\text{O}_{19}$ ). X-ray powder diffraction was used to carry out the quantitative analysis of phases and to determinate the crystallographic parameters. It was found that the compound consists of only one phase and that the coercivity, remanence and saturation increased with the strontium content. The initial susceptibility was also obtained and results are discussed in terms of the magnetization mechanisms produced by the effect of the substitution on the hexaferrite. Furthermore, Néel temperature measurements indicate a strengthening of the exchange interactions with increasing strontium content.

Keywords: M-type hexaferrite, Magnetic properties, Rietveld refinement, Cationic substitution.

### **Introduction**

M-type hexaferrites are one of the most interesting materials due to its wide variety of properties that present, most of them, simultaneously. It is well known that M-type hexaferrite presents ferrimagnetism [1], but it has also been reported to exhibit electrical [2, 3], photocatalytical [4], magnetocalorical [5] and microwave absorbing [6] properties. Some of these properties depend on factors such as the preparation method



i.e. on the shape and particle size. Substitutions have modified the intrinsic extrinsic properties of the hexaferrites [7–11]; when substitution is carried out, the crystal structure changes due principally to the difference in ionic radii and valence of the cations involved and the magnetic properties changes because the super-exchange interactions between iron ions are modified. The substitutions also modify the spin canting angle, which is responsible of changes in the electrical properties e.g. DC electrical resistivity ( $\rho$ ) or the drift mobility ( $\mu_d$ ) [12].

A study of the properties of the  $\text{Pb}_{0.5}\text{Sr}_{0.5}\text{Fe}_{12-x}\text{Pb}_x\text{O}_{19}$  compound was reported in a previous paper [13]; however, it was not possible to obtain the pure phase in that system because it was not considered the lead evaporation [14]. Thus the measured properties may have been influenced by the presence of secondary phases.

In this work the best conditions were found to make possible the substitution of lead by strontium in the hexaferrite prepared by means of the ceramic method.

Since lead evaporates around 900 °C, a quantitative analysis of phases was made to determine the quantity of lead precursor necessary to compensate the lead loss [14]. The sintering temperature ranges from 1000 °C to 1200 °C, in intervals of 50°C. The hexaferrite structure is obtained without secondary phases for all compositions assuming that lead and strontium share the same site in the crystal lattice.

This fact, as far as is known by the authors, has not been reported yet.

The characterization of the samples was made in order to determinate the influence of the substitution on the properties of the samples. The structural characterization was performed by X-ray diffraction using a GBC Enhanced Mini-Materials Analyzer diffractometer with  $\text{Cu}(\text{K}\alpha)$  radiation in Bragg–Brentano geometry.

The MAUD program [15, 16], which includes the Rietveld algorithm, has been used for the refinement of the crystal structure and for the quantification of phases, carried out at every step of the preparation. The magnetic characterization was performed with a Micromag 2000 vibrating sample magnetometer with  $H_{\max} = 12$  KOe in order to obtain the magnetic saturation ( $\sigma_s$ ), the magnetic remanence ( $\sigma_r$ ), the coercive field ( $H_c$ ), and the initial susceptibility ( $\chi_i$ ). The Néel temperature also has been determined by using the magnetic-TGA technique and the morphology of the samples was observed with a Jeol 1200 scanning electron microscope working at 120 kV.

## Experimental

Polycrystalline M-type substituted hexaferrite ( $\text{Pb}_{1-x}\text{Sr}_x\text{Fe}_{12}\text{O}_{19}$ ,  $x = 0.1, 0.3, 0.5, 0.7$  and  $0.9$ ) was obtained by the ceramic method using, as chemical precursors, lead oxide ( $\text{Pb}_3\text{O}_4$ ); strontium carbonate ( $\text{SrCO}_3$ ) and hematite ( $\alpha\text{-Fe}_2\text{O}_3$ ), all of them of analytical grade. In the first stage of the preparation, the powders were weighed according to the stoichiometric chemical reaction; the powders were mixed in ethylic alcohol for one hour in a rotary mill at 90 rpm; later, the powders were dried at  $50^\circ\text{C}$ , and presintered at  $800^\circ\text{C}$  for one hour; at the second stage of the preparation, the lead, lost during the heat treatment by evaporation, was compensated by adding lead oxide; this amount is constant (33.9%) for all compositions [17], the excess of lead oxide was mixed in ethylic alcohol with the presintered powders for one hour. The resultant powders were compacted applying an axial load of  $2.5\text{ T/cm}^2$  on cylindrical samples of 4.8 mm in diameter. Finally, the samples were sintered at  $1100^\circ\text{C}$  during 60 min and cooled slowly in the furnace.

## Results and discussion

X-ray diffractograms of all samples were recorded and then analyzed with the Rietveld refinement method in order to obtain the structural parameters for each composition. The models used for the refinement were constructed on basis of the lead hexaferrite (hexagonal; space group P 63/mmc) with  $a = 5.902 \text{ \AA}$  and  $c = 23.207 \text{ \AA}$  [14]. The  $\text{Sr}^{2+}$  was placed at the  $\text{Pb}^{2+}$  site in a fraction according to the  $x$  value, so the occupation of both contributions always is the unity.

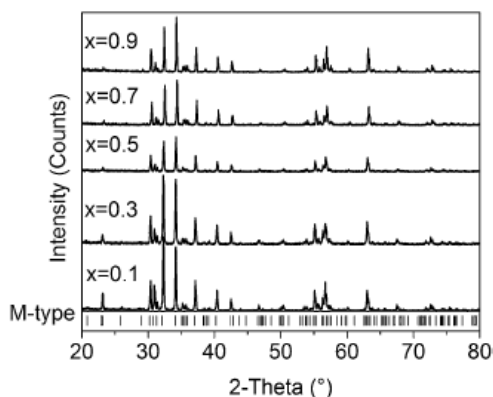


**Fig. 1** X-ray powder diffractograms of lead hexaferrite substituted with strontium;  $x$  indicates the strontium content

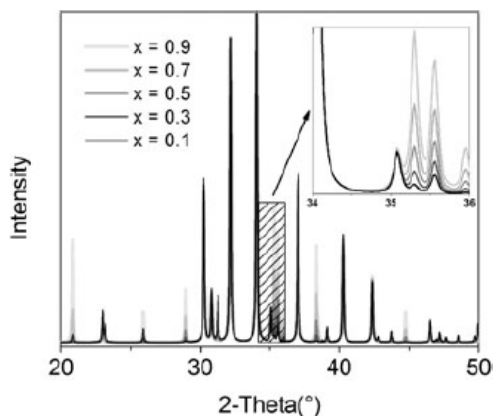


**Fig. 2** Theoretical diffractograms calculated for  $\text{Pb}_{1-x}\text{Sr}_x\text{Fe}_{12}\text{O}_{19}$ ; with  $x = 0.1, 0.3, 0.5, 0.7$  and  $0.9$ . The *inset* shows variations in the intensity of the peaks between  $34^\circ$  and  $36^\circ$  as the strontium content varies

Figure 1 shows the X-ray diffractograms. At the bottom, the positions of the reflections are shown, corresponding to the M-type hexaferrite structure; Rietveld refinement results showed how the structural parameters change as the strontium content changes, Table 1. The refinement program adjusts the theoretical model to the experimental data by taking in account the crystalline and instrumentals parameters. A simulation of the X-ray patterns as a function of strontium content in the substituted samples was made using the CCDC Mercury program, Fig. 2. The intensity of the peaks is a function of the atomic structure and depends on factors such as the ionic scattering factor and the structure factor that, in turn, depends on the population factor and is related with the occupancy of sites by the corresponding atoms. During the atomic substitution the occupation occurs of the same position of the unit cell with two different kinds of atom (strontium and lead). This causes locally differences of the environment although the volumes and electronic properties of the atoms are similar; thus, the differences in intensity of the calculated diffractograms could be attributed to variations in the closer environment of the substituted sites.

Sr (x)	Unit cell parameters (Å)		Cell volume (Å <sup>3</sup> )	Cryst. size (nm)	X-ray density (g/cm <sup>3</sup> )	Pb occ	Sr occ
	a	c					
0.1	5.9031 (1)	23.1568 (4)	807	278 (2)	5.726	0.88 (1)	0.09 (2)
0.3	5.8997 (1)	23.1379 (3)	805	289 (9)	5.483	0.69 (0)	0.29 (1)
0.5	5.8958 (1)	23.1128 (4)	803	401 (4)	5.329	0.49 (1)	0.49 (1)
0.7	5.8945 (5)	23.0952 (9)	802	513 (34)	5.235	0.29 (0)	0.69 (1)
0.9	5.8919 (0)	23.0768 (2)	801	750 (80)	5.140	0.10 (0)	0.89 (1)

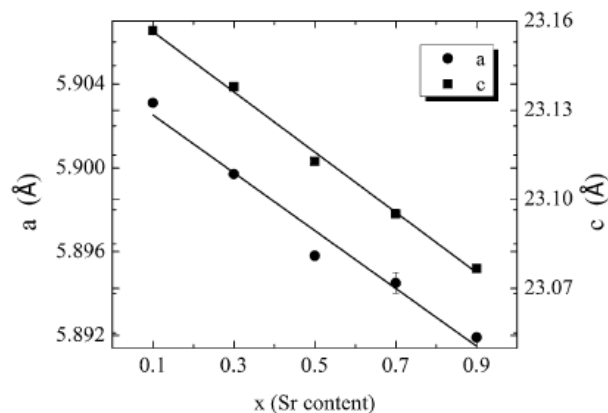


Fig. 3 Cell parameters,  $a$  (●) and  $c$  (■) of the substituted strontium hexaferrite

The experimental X-ray results show that by increasing the strontium content, the lattice parameters tend to decrease linearly, Fig. 3. This behavior and the results of occupancy, composition of phases and crystal structure obtained from X-ray characterization indicates that the strontium and lead occupies the same site in the crystal structure and both enter homogeneously forming a complete solid. On the other hand, the increase of the strontium content in the hexaferrite produces an increase in the crystallite size and a reduction in the particle size, as shown the SEM micrographs and particle size distribution graphs of Fig. 4. The particle size distribution was measured from SEM micrographs over 300 particles with a magnification of 5000 $\times$ . Samples with  $x = 0.9$  and  $0.5$  have a uniform morphology of small rounded particles with a narrow particle size distribution and mean particle size of  $0.62 \mu\text{m}$  for  $x = 0.9$  and  $0.83 \mu\text{m}$  for  $x = 0.5$ . In the samples with  $x = 0.3$  and  $0.7$  an inhomogeneity was found in the particle size distribution, however, both samples exhibit the same behavior, the mean particle size is about  $1 \mu\text{m}$  and the grains tend to be flattened. In the case of the sample with  $x = 0.1$ , the typical hexaferrite morphology (hexagonal plates) is present and the

average particle size determined for this composition is 2.43  $\mu\text{m}$ . According to these results, the substitution with strontium should inhibit the grain growth in the samples this may be due an increase in lattice defects such as stacking faults, which block the growth of the grains.

The magnetic properties of all the samples were obtained at room temperature by measuring the magnetization curves, Fig. 5. The most evident change is observed on the coercive force,  $H_c$ , which varies from 1.57, for  $x = 0.1$ , to 4.27 kOe for  $x = 0.9$ ; the remanence,  $\sigma_r$ , rises from 31.2 to 42.2 emu/g and the magnetic saturation,  $\sigma_s$ , varies from 68.1 to 69.1 emu/g, Fig. 6. The sample with  $x = 0.9$  presents a noticeable remanence-enhancement effect as shown by the  $M_r/M_s$  ratio in comparison with the sample with higher content of lead which resulted in a value below  $0.5 M_s$ , which is the limit value for non-interacting particles [19]. Table 2 shows results of the magnetic characterization.

The presence of structural defects or disorder plays a dominant role on the magnetization curves and on the determination of the initial susceptibility  $\chi_{in}$ , which is one way to characterize hard magnetic materials. From the behavior of the initial curve of magnetization with increasing applied magnetic field, it is possible to determine the different types of magnetization process in the linear region of the virgin curve.

The initial susceptibility of all the samples was obtained from (1) [18]:

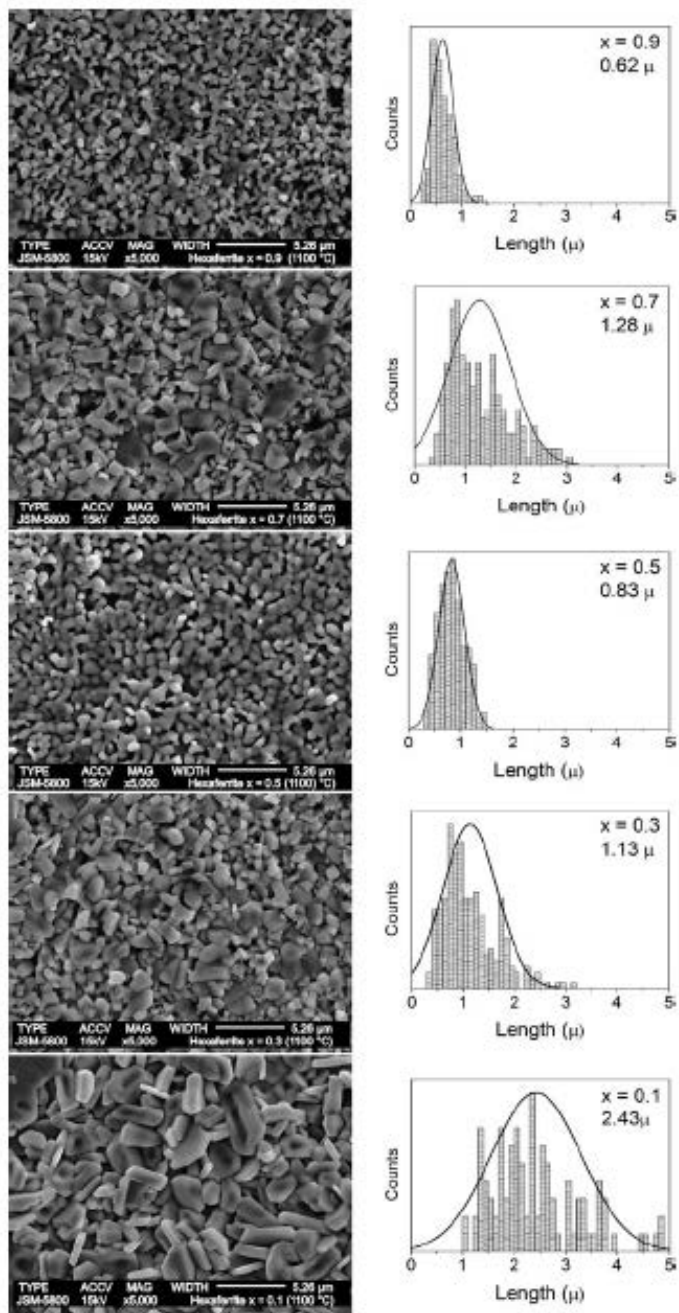
$$M = \chi_{in} H_a. \quad (1)$$

Figure 7 shows a reduction in initial susceptibility when the content of strontium decreases, indicating that for high content of strontium ( $x = 0.9$ ), the pinning mechanism

of the walls motion is favored; when the applied field increases, and the domain structure has been swept away, prevail the nucleation of reversed domains that hinder the magnetization process. On the other hand, for low contents of strontium ( $x = 0.1$  and  $0.3$ ), the mechanisms of nucleation of inverse domains are favored; that is, the virgin curve is steeper and saturation is reached first, here the domain walls moves due to the reduced pinning effects [19].

The strontium incorporation into the crystal structure is supported by Néel temperature,  $T_N$ , measurements. This is one of the most sensitive parameters to demonstrate that the substitution was carried out. The transition temperature from ferrimagnetic to paramagnetic was determined and Fig. 8 shows the Néel temperature, which varies linearly with composition,  $x$ .

**Fig. 4** Micrographs at 5000 $\times$  and particles size distribution of the substituted hexaferrite



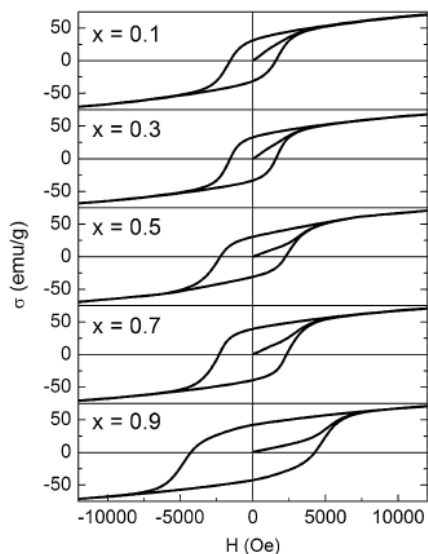


**Fig. 5** Hysteresis loops obtained at room temperature with different strontium content

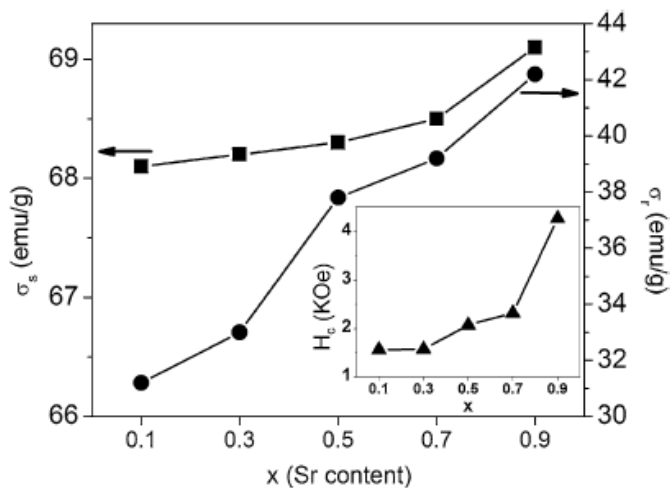


**Fig. 6** Properties obtained from the magnetic characterization; magnetic saturation (■), magnetic remanence (●) and coercive force (▲)

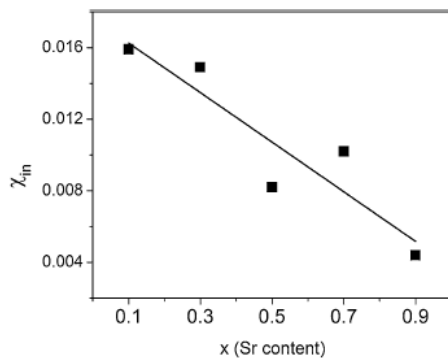


Fig. 7 Initial susceptibility calculated from the virgin curve of the hysteresis loop

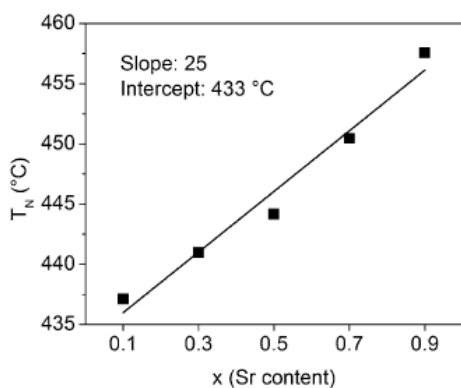


Fig. 8 Measurement of Néel temperature as a function of strontium concentration. The interception indicates the Néel temperature of the pure lead hexaferrite [20, 21]

**Table 2** Results of the measurements of the magnetic parameters

Sr content ( <i>x</i> )	$\sigma_s$ (emu/g)	$\sigma_r$ (emu/g)	$H_c$ (kOe)	$M_r/M_s$	$T_N$ (°C)	$J$ (eV)
0.1	68.0	31.2	1.57	0.44	437.1	0.0918
0.3	68.2	33.0	1.58	0.48	440.9	0.0923
0.5	68.3	37.8	2.08	0.55	444.2	0.0927
0.7	68.5	39.2	2.32	0.57	450.4	0.0935
0.9	69.1	42.2	4.27	0.61	457.5	0.0944

The exchange interactions between sites *i* and *j* are estimated according to the average exchange parameter  $J_i = \sum_{i \neq j} J_{ij}$ . The mean field theory was used to

approximate the average exchange parameter, (2), which is related with the exchange interaction due to the super-exchange coupling between iron ions [22].

$$J_i = (3/2)kT_N \quad (2)$$

where  $k$  is the Boltzmann constant.

The results of average exchange parameter  $J_i$  are listed in Table 2 as a function of the strontium content; this indicates that the exchange interactions, which are responsible of the ferrimagnetic coupling, were modified when strontium enters into hexaferrite structure; in this sense, it occurs that the strontium tend to produce a unit cell slightly smaller than the unit cell with lead (see Table 1), and the super-exchange coupling of iron ions is stronger when the distance of the super-exchange decreases.

### **Conclusion**

Pure phase of hexaferrite was obtained substituted with strontium and lead, for all range of compositions according to the chemical equation  $Pb_{1-x}Sr_xFe_{12}O_{19}$  and prepared using the ceramic method. The key in obtaining pure phase lies in accurate determination of the quantity of lead loss during the preparation. It was found, from the Rietveld refinement results, that the crystal parameters vary linearly according to the strontium concentration and the simulated X-ray powder diffraction patterns show variations in intensity which are produced as an effect over the closer environment of the strontium substitution in the unit cell; this produces slight changes in the arrangement of atoms and changes their interatomic distances which results in changes in the intrinsic properties of the hexaferrite.

The extrinsic magnetic properties show a dependency with strontium content variation; for example, in the case of remanence and saturation, this dependence is linear and increases with increasing strontium, but in the case of coercivity, this increase is exponential. From the initial susceptibility it was possible to discuss which could be the magnetization mechanisms at low magnetic fields. It was found that high content of strontium favors the pinning of the domain walls, while for high lead concentration ( $x = 0.1$  and  $0.3$ ), the prevailing mechanism is the rotation of inverse domains. There was not found a direct correlation between the magnetic properties and microstructure; however, the microstructure tends to be modified according the concentration of strontium; in the same way, the strontium could act as a grain growth inhibitor perhaps by the formation of stacking faults since there are no inclusions or secondary phases that inhibit the growth of grains.

We have a correlation between the length of the unit cell with the degree of substitution and the intrinsic magnetic properties, through the exchange parameter  $J_i$ , which is a measure of the average exchange interactions. The unit cell size diminishes as the strontium concentration increases, when that occurs, a diminishing in the exchange lengths is expected and the super-exchange couplings between iron sites are stronger.

### **Acknowledgements**

We would like to thank CONACYT (México) for support given to carry out this work. Thanks are also due to Gerardo-López and A. Encinas-Oropesa.

### **References**



1. Litsardakis, G., Manolakis, I., Serletis, C., Efthimiadis, K.G.: J. Magn. Magn. Mater. 310, 2006–2008 (2007)
2. Javed-Iqbal, M., Naeem-Ashiq, M., Hernandez-Gomez, P., Muñoz, J.M.: J. Magn. Magn. Mater. 320, 881–886 (2008)
3. Novák, P., Knížek, K.: J. Magn. Magn. Mater. 316, e587–e590 (2007)
4. Hessien, M.M., Khedr, M.H.: Mater. Res. Bull. 42, 1242–1250 (2007)
5. Hamam, Y.A., Said, M.R., Abu-Aljarayesh, I.: Physica B 321, 129–132 (2002)
6. Lixi, W., Qiang, H., Lei, M., Qitu, Z.: J. Rare Earths 25, 216–219 (2007)
7. Wang, L., Qiang, H., Lei, M., Qitu, Z.: J. Rare Earths 25, 216–219 (2007)
8. Wang, J.F., Ponton, C.B., Harris, I.R.: J. Magn. Magn. Mater. 234, 233–240 (2001)
9. Litsardakis, G., Manolakis, I., Serletis, C., Efthimiadis, K.G.: J. Magn. Magn. Mater. 316, 170–173 (2007)
10. Bercoff, P.G., Herme, C., Jacobo, S.E.: J. Magn. Magn. Mater. 321, 2245–2250 (2009)
11. Ounnunkad, S.: Solid State Commun. 138, 472–475 (2006)
12. Javed, M., Naeem, M., Hernandez-Gomez, P., Maria, J.M.: J. Magn. Magn. Mater. 320, 881–886 (2008)
13. Hussain, S., Shah, N.A., Maqsood, A., Ali, A., Naeem, M., Ahmad Adil Syed, W.: J. Supercond. Nov. Magn. 19, 6–9 (2011)
14. Palomares-Sánchez, S., Díaz-Castañón, S., Ponce-Castañeda, S., Mirabal-García, M., Leccabue, F., Watts, B.: Mater. Lett. 59, 591–594 (2005)
15. Ferrari, M., Lutterotti, L.: J. Appl. Phys. 76, 7246–7255 (1994)

16. Will, G.: The Rietveld Method and the Two Stage Method to Determine and Refine Crystal Structures from Powder Diffraction Data. Springer, Berlin (2006)
17. Guerrero-Serrano, A.L., Pérez-Juache, T.J., Mirabal-García, M., Matutes-Aquino, J.A., Palomares-Sánchez, S.A.: J. Supercond. Nov. Magn. 24, 2307–2312 (2011)
18. Becker, J.J.: IEEE Trans. Magn. 12, 965–967 (1976)
19. Bertotti, G.: Hysteresis in Magnetism. Academic Press, San Diego (1998)
20. Albanese, G., Díaz-Castañón, S., Leccabue, F., Watts, B.E.: J. Mater. Sci. 35, 4415–4420 (2000)
21. Albanese, G., Leccabue, F., Watts, B.E., Díaz-Castañón, S.: J. Mater. Sci. 37, 3759–3763 (2002)
22. Cullity, D.B., Graham, C.D.: Introduction to the Magnetic Materials. Addison Wesley, Reading (2009)